Journal of Materials Education Vol. 34 (3-4): 69 - 94 (2012)

THE NATURE OF THE GLASSY STATE: STRUCTURE AND GLASS TRANSITIONS

Ioannis M. Kalogeras [1,2] and Haley E. Hagg Lobland [2]

[1] Section of Solid State Physics, Department of Physics, University of Athens, Panepistimiopolis, Zografos 157 84, Greece; *ikaloger@phys.uoa.gr, im.kalogeras@gmail.com*.

[2] Laboratory of Advanced Polymers & Optimized Materials, (LAPOM), Department of Materials Science & Engineering and Department of Physics, University of North Texas, 1155 Union Circle #305310, Denton, TX 76203-5017, USA; *haleylobland@gmail.com*.

Key words: *crystals, glasses, polymer composites, amorphous structure, glass transition, free volume, Voronoi tessellation, binary radial distribution function*

ABSTRACT

Materials in the glassy state have become an increasing focus of research and development and are found in a variety of commercial products and applications. While non-crystalline materials are not new, their often unpredictable properties and behavior continue to elude neat systems of classification. For purposes of teaching, there is presently a need for further explication of glasses, especially given their high importance and the wide extent of glassy materials in existence. This work is thus intended to address that need. Voronoi polyhedra have been used to represent amorphous (glassy) structures with considerable success; however, the system and procedure are not well taught and understood as, for example, are Miller Indices for describing crystals. The present article provides a practical update on results extracted from Voronoi polyhedra analyses of simulated and real physical systems. There is an alternative approach to characterization of amorphous and liquid structures, namely the binary radial distribution function, which is explained. Above all this article discusses the nature of the glassy state.

INTRODUCTION

In the earliest approaches – dating back to the Bronze and Iron Age – the atomic structures of naturally occurring crystalline materials were amended by introducing lattice defects, e.g. by forging. Nowadays, in a century of tremendous industrial and technological growth, the majority of solid materials already in use or under evaluation for novel applications are in a non-crystalline state[1,2]. In spite of that, instruction in Materials Science and Engineering (M.S.E.) and in related disciplines remains largely focused on crystals. An attempt to remedy this situation was made in this Journal just more than a decade ago, in an article

explaining the representation of amorphous structures by Voronoi polyhedra and underlining their effectiveness in isolating even subtle differences among the possible physical states of a system[3]. Changes in several metric properties of a Voronoi polyhedron –which is defined as the convex region of space closer to its central particle (ion, atom, molecule, monomer, chain segment, etc.) than to any other– convey information on microstructural fluctuations of various causes. There are in fact two methods of characterization of amorphous materials; the second one is based on binary radial distribution functions. Both approaches are discussed in the remainder of this article. To begin, we address the fundamental distinctions between glasses and crystals and between the glassy and liquid states.

GLASSES *vs.* CRYSTALS

As a liquid is cooled from a high temperature, it may either crystallize (at the melting temperature T_m) or become super cooled; this is shown by the temperature dependence of the specific volume, entropy or enthalpy, under constant pressure, as illustrated in Fig. 1a. The particles (atoms, molecules or ions) forming crystalline materials are arranged in orderly repeating patterns, with elementary building blocks (unit cells) extending to all three spatial dimensions. The structures of crystalline solids depend (predictably) on the chemistry of the material and the conditions of solidification (starting temperature and cooling rate, ambient pressure, etc.), and can be described easily in detail by combining crystallographic notions with diffraction/scattering data[4-6]. Super cooled liquids, on the other hand, demonstrate a rather intriguing behavior. Upon further cooling below the T_m, their particles progressively lose translational mobility, so that around the so-called glass transition temperature (T_g) rearrangement to "regular" lattice sites is practically unfeasible; this behavior is distinctive for the amorphous structures described as glasses or vitreous solids.

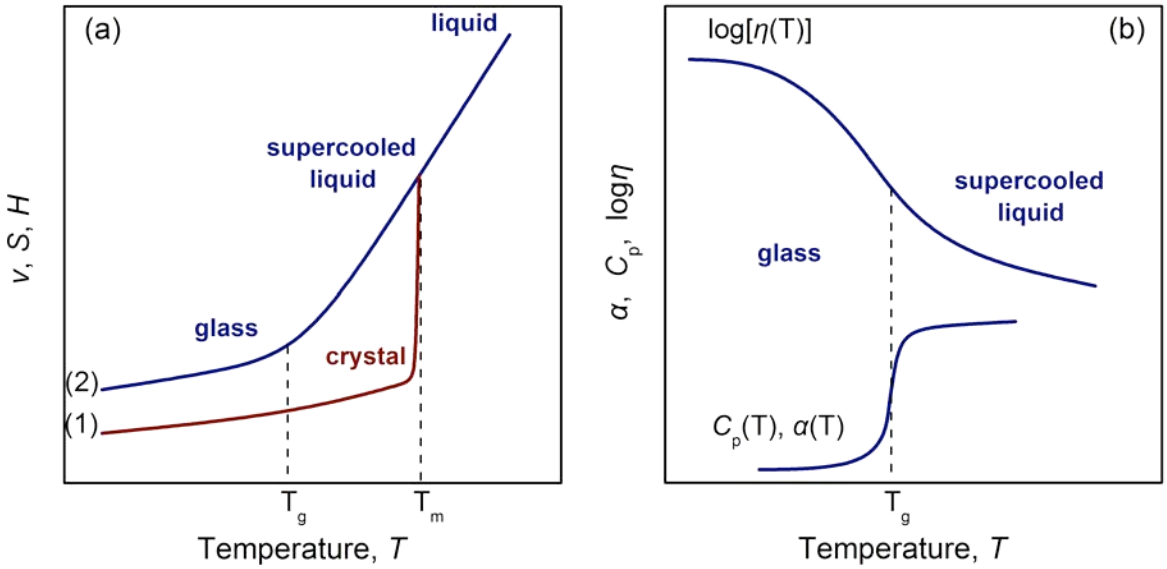

Figure 1. (a) Typical temperature dependence of the specific volume (v), entropy (S), or enthalpy (H) of glasses and crystals. Path (1) is not possible in, for example, atactic polymers lacking a crystalline ordering state. (b) Temperature dependence of the isobaric expansivity (also called coefficient of thermal expansion) [$\alpha = V^{-1}(\vartheta V/\vartheta T)_P$], heat capacity [$C_p = (\vartheta H/\vartheta T)_P$], and $\log_{10}$ of viscosity (η), in the region of T_g.

The term liquid-glass transition –frequently abbreviated to glass transition– signifies the reversible transition in amorphous materials (including amorphous regions within semi crystalline materials) from a molten or rubber-like state into a hard and relatively brittle state. The question of what phase transition underlies the glass transition is a matter of continuing research. Evidently, this process bears no connection with the first-order phase transitions in Paul Ehrenfest's (1933) classification scheme[7]. Those exhibit a discontinuity in the first derivative of the Gibbs energy (G) with respect to some thermodynamic variable: crystallization proffers a characteristic example, as discontinuities emerge in both density and specific volume ($v = (\partial G/\partial P)_T$, P = pressure) versus temperature (T) plots. On the other hand, it is observed in glasses that intensive thermodynamic variables such as the thermal expansivity and heat capacity (second-order derivatives) exhibit a smooth step (formally a discontinuity at T_g) upon cooling (or heating) through the glass transition range (Fig. 1b). This fact supports connections of the glass transition phenomenon with a second-order phase transition[8]. Nevertheless, the glass transition is *not* a transition between states of thermodynamic equilibrium: it is widely believed that the true equilibrium state is always crystalline. Only by annealing or ageing (when time, t, constitutes the prime experimental parameter) is structural relaxation facilitated and the structure enabled to explore lower energy minima – inaccessible during the cooling process – allowing a progressive shift to a more stable (lower energy and entropy) state. Given the fact that the glass transition is dependent on the history of the material (e.g., see Figure 2)[8] and on the rate of temperature change, it seems reasonable to consider it as merely a dynamic phenomenon, extending over a range of temperatures and defined by one of several conventions[9].

Interestingly, different operational definitions of the glass transition temperature are in use, and several of them are endorsed as scientific standards. For example, in rheological studies one considers T_g to be the temperature at which

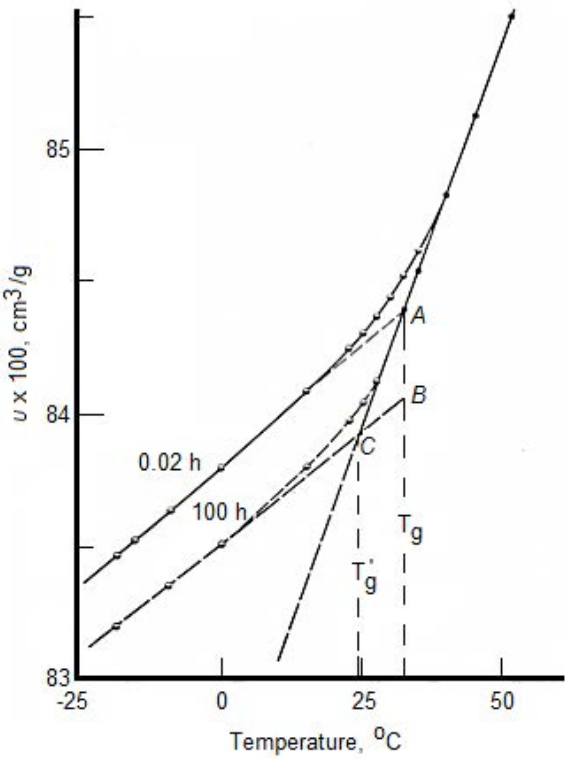

Figure 2. A kinetic feature of the glass transition phenomenon demonstrated in the temperature variation of the isobaric volume of polyvinyl acetate. Black dots represent equilibrium volumes, while the half-moons correspond to the volumes observed 0.02 h and 100 h after sample quenching (adapted from Ref. 10).

system's viscosity reaches the threshold of $\eta = 10^{13}$ Poise (10^{12} Pa·s), an unfounded supposition. In dilatometric studies the glass transition temperature is located at the intersection between the cooling $V - T$ curve for the glassy state and the super cooled liquid (Fig. 1a), which typically gives a value of the T_g approximately equal to $2T_m/3$; a feature recognized[11] as early as 1952 and applauded[12] as "a good empirical rule" with the addition that "symmetrical molecules such as poly(vinylidene chloride) tend to have ratios about 0.06 smaller than unsymmetrical molecules such as polypropylene".[12] In dynamical experiments, such as in isothermal dielectric spectroscopy studies (where a frequency- and time-dependent electric field $E(\omega, t)$, the *stimulus*, interacts with the electric dipoles in a many-particle system), T_g is defined as the temperature where the

"structural" relaxation time (τ) reaches the value 100 s. In such experiments, τ pertains to the time-scale of system's shift to equilibrium after, for example, a thermal, mechanical or electrical perturbation[9]; structural relaxation (or intermolecular rearrangement) proceeds by collective motions of structural elements (ions in metallic glasses, and chain segments in amorphous polymers, etc). Even in the case of differential scanning calorimetry (DSC), which is a routine thermal analysis method[9], one will find several definitions of T_g. All these arbitrary definitions generate largely dissimilar estimates; at best, values of T_g for a given substance agree within a few Kelvin. Multiple glass transitions may appear in multiphase (composite) systems, providing information on the state of mixing and the strength of interaction between the components.

As the liquid passes through its T_g during cooling, its viscosity increases by as much as 17 orders of magnitude (Fig. 1b), but static structural parameters (e.g., the static structure factor[13], $S(q)$) change almost imperceptibly. The absence of long-range order is a distinctive – but not the only – difference between glasses and crystals. The glass exhibits a long-range structure close to that observed in the super cooled fluid phase, while displaying solid-like mechanical properties on the timescale of practical observation. Both in a glass and in a crystal it is only the vibration degrees of freedom and some rotational motions that remain active whereas translational motion is arrested.

GLASSES *vs.* LIQUIDS

Having discussed the features distinguishing glasses from crystals, we now address the distinctions between the glass and liquid states. We are familiar generally with the differences between a liquid and a glass. However, for certain purposes the existing analytical techniques do not provide sufficient structural details to quantitatively distinguish glass from a liquid phase. The molecular processes governing the translation of a liquid into a rigid amorphous solid are not yet well understood and are therefore still a subject of much research.

Consider again, what happens during the glass transition. Refer to Fig. 1a: upon cooling below T_m, molecular motion slows, and below T_g the rate of change of volume (or enthalpy) decreases to a value similar to that of the crystalline solid. Since slower cooling rates allow a longer time for particles to sample different configurations (maintaining the liquid-state equilibrium longer), the value of the T_g necessarily decreases with a slower rate of cooling. Additionally, viscosity (as well as the structural relaxation time) is very sensitive to temperature near the T_g: some liquids exhibit a significant viscous slow-down near the glass transition, presumably owing to relaxation processes. Although it has been reported that the Vogel-Tammann-Fulcher-Hesse (VTFH) equation[14,15]

$$\eta(T), \tau(T) \propto \exp\left(\frac{C}{T - T_0}\right) \qquad (1a)$$

(where C is a system-specific constant) represents this behavior reasonably well[16], it was later stated[17] that "there is no compelling evidence for the VTFH prediction that the relaxation time diverges at a finite temperature". In a separate attempt to model the behavior of super cooled liquids, Angell used fragility plots (Angell plots), where the logarithm of a dynamical quantity (commonly, η or τ) are plotted versus T_g/T (e.g., see Fig. 3), to classify liquids on a scale from strong to fragile[18-20]. In Angell's classification scheme the word "fragility" is used to determine the tendency of materials to form glasses, in contrast to its colloquial meaning, which more closely relates to the brittleness of a solid material. Formally, fragility reflects to what degree the temperature dependence of the viscosity, relaxation time, or the resistivity of the glass former, deviates from the Arrhenius behavior; strong glass-formers nearly exhibit an Arrhenius-type dependence

$$\eta(T), \tau(T) \propto \exp\left(\frac{C}{T}\right) \qquad (1b)$$

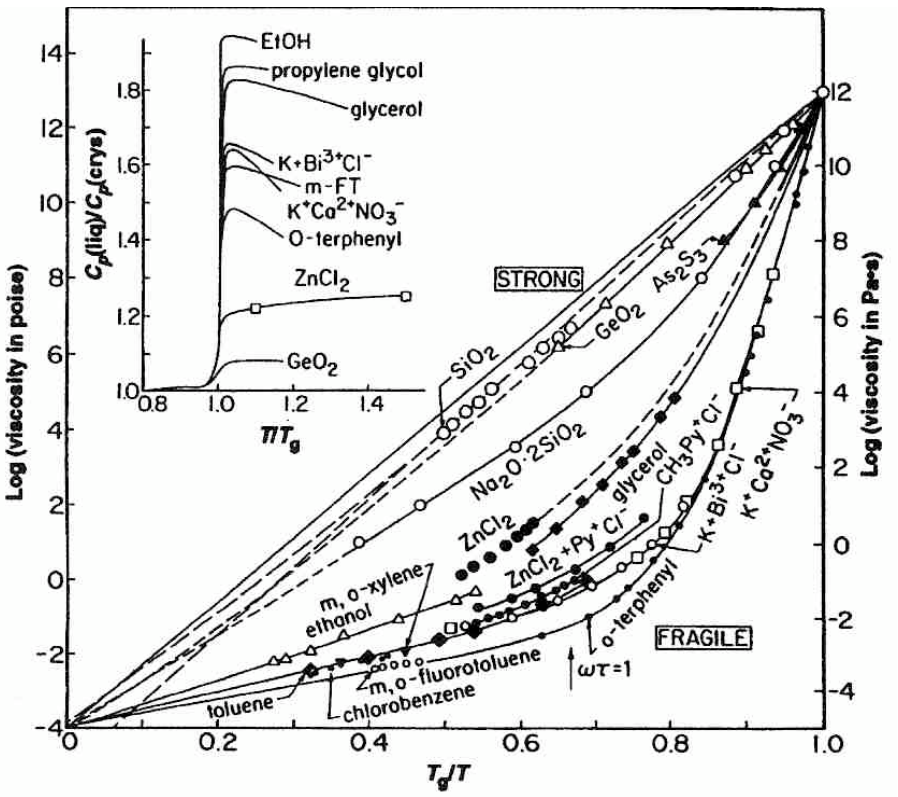

Figure 3. Fragility (or Angell) plots: logarithm of viscosity (log η) vs. reduced temperature (T_g/T) plot for glass forming liquids. Inset: heat capacity change at the glass transition for selected systems.[20]

which implies a simple thermally-activated behavior. Moreover, according to this classification, liquids are also distinguished by their structures: strong liquids such as SiO_2 and GeO_2 (network oxides) have tetrahedrally coordinated structures while non-directional dispersive forces and complex coordination are characteristic of molecules in fragile liquids (such as *o*-terphenyl). The classification of liquids as strong versus fragile glass-formers is one that continues to be used and continues as a subject of investigation. Apart from providing a relationship to viscosity behavior, the classification system provides for some correlation to structural features, although we shall see later there are alternative approaches to such relationships.

Other changes observed in liquids at temperatures near the glass transition temperature seem to provide additional clues for distinguishing the glassy state from the liquid state. There appears a decoupling between translational diffusion and viscosity and also between rotational and translational diffusion that occurs below approximately $1.2T_g$.[16] Proportionality between the said properties is evident at higher temperatures but no longer holds as the glass transition is neared. Isothermal dielectric relaxation studies of some materials indicate that at sufficiently high temperatures the liquid exhibits a single relaxation mechanism, while at moderate super cooling the liquid may exhibit two different relaxation mechanisms[16]. Such observations highlight the importance of Arrhenius plots (i.e. $\tau(T)$ vs. T^{-1} plots) in studies of system dynamics and their potential effectiveness for distinguishing the glassy and liquid states; and we shall see later how a geometrical approach may be used to that end.

We cannot leave such a discussion without mention of thermodynamics. Important in the present analysis is entropy, especially as it is possible to calculate the entropy difference

between the (super cooled) liquid and crystalline states. At the melting temperature, entropy of the liquid state is higher than that of the corresponding crystal. The difference between the two decreases with the temperature owing to higher heat capacity of the liquid state. (Importance of the heat capacity function is addressed elsewhere by Angell[21].) It would seem from this trend that the entropy difference would soon vanish, however the kinetics of the glass transition intervene[16]. It has therefore been proposed that the glass transition is a "kinetically-controlled manifestation of an underlying *thermodynamic transition* to an ideal glass with a unique configuration".[16] A formula of Adam and Gibbs promotes this connection[22]:

$$\eta(T),\tau(T) \propto \exp\left(\frac{C}{T \cdot S_c}\right) \qquad (1c)$$

where C is again a system-specific constant, and S_c is the configurational entropy. The Adam-Gibbs theory provides a picture of the behavior leading to the glass transition. According to this theory, a decrease in the number of available configurations that the system can sample leads to a viscous slow-down (mentioned earlier) close to the transition temperature[16]. Adam and Gibbs invoke the idea of cooperatively rearranging regions (CRRs) in their derivation of Eq. (1a) but do not indicate the size of such regions nor provide a means to distinguish CRRs from one another. In spite of the aforementioned weakness in the Adam-Gibbs theory, Eq. (1a) describes the behavior of super cooled liquids quite well. Furthermore the outworking of the theory suggests an important connection between dynamics and thermo-dynamics and also between kinetic fragilities and thermodynamic fragilities[16].

Super cooled liquids and the glass transition can also be considered from the viewpoint of the potential energy landscape. The so-called energy landscape picture provides a convenient framework within which to interpret existing data and purported concepts. Further details of the system are discussed later in this review. In brief, the landscape picture establishes molecular motion at low temperatures as sampling distinct potential energy minima, with further distinction of vibrations within a minimum. A formal separation of configure-tional and vibrational contributions to a liquid's properties is therefore possible[16]. Another interesting idea coming out of the landscape picture is the notion that super cooled fragile liquids are dynamically heterogeneous: possibly consisting, in instantaneous moments, of mostly non-diffusing molecules with just a few 'hot spots' of mobile molecules, a theory evidently supported by experimental and computational work[16]. Also noteworthy of the landscape view-point is that it gives a conceivable interpretation for the decoupling of the primary (α) and secondary (β) dynamic mechanical and dielectric relaxation modes, originating, respectively, from cooperative (long-range) and weakly or non-interacting (localized) motions of structural units.

The glass transition phenomenon is often treated also as a *purely dynamic transition*; there is no singularity, except that with decreasing temperature the dynamics become so slow that the system behaves as a solid. The most famous approach of this kind is the mode-coupling theory (MCT), which describes a non-linear feedback mechanism that links shear-stress relaxation, diffusion, and viscosity. The result of this would be structural arrest occurring as a dynamic singularity[16]. Although some features of relaxation dynamics of liquids are described well by MCT, it does not give us a theory of the glass transition and therefore a particular means of predicting the transition from liquid to glass.

In summary, we have not yet arrived at a coherent theory of super cooled liquids and glasses. The behavior of many liquids near the glass transition has been described, but not all that behavior is thoroughly explained. In their review of the topic Debenedetti and Stillinger[16] posit that the energy landscape perspective can explain *qualitatively* much of the behavior. What remains then is to establish theoretical perspectives with quantitative support. Related attempts should be –at least in part– built on the dissimilarities existing between liquid and

glassy structures, which can be described by means of the mathematical concepts of the radial distribution function and the Voronoi polyhedra.

THE RADIAL DISTRIBUTION FUNCTION FOR SPATIAL DESCRIPTION OF NONCRYSTALLINE SYSTEMS

Having spent some considerable time discussing the nature of the liquid, glass, and crystalline states with regard to their physical properties and behaviors, we now advance to discussion on spatial descriptions of amorphous systems. Our picture of glassy structures has considerably improved – and given shape beyond the instructive balls and sticks model– by detailed images of Monte Carlo (MC) and molecular dynamics (MD) computer simulations of amorphous cells[23]. The mathematical concept of the radial distribution function (RDF) $g(r)$, also known as the pair correlation function[3,24,25], has provided a means for distinguishing subtle differences among the amorphous solid and liquid states of matter[26], especially with regard to structure.

The binary radial distribution function is a measure of the probability, $\rho^{2/N}(0, r)$, of finding a particle within an arbitrary reference frame and located in a spherical shell of an infinitesimal thickness at some distance r from a reference center[13]. That is, the RDF is defined as

$$g(r) = \rho^{2/N}(0,r)/\rho^2 \qquad (2)$$

where $\rho = N/V$ is the average number density of N-particle system (e.g., a fluid) in a container of volume V. $\rho g(r)4\pi r^2 dr$ is the number of particles at a distance between r and $r + dr$. The calculation of $g(r)$ involves averaging the number of particles at a distance r from any particle in the system and dividing that number by the element of volume $4\pi r^2 dr$. It is thus possible to measure $g(r)$ experimentally with neutron scattering[27] or x-ray scattering diffraction[28] data, or by simply extracting the positions of large enough (micron-sized) particles from microscopy techniques (e.g., tranditional or confocal microscopy[29]). In addition, given a pair potential energy function $u(r)$, the RDF can be found either via computer simulation methods or through approximate functions[30]. Relations involving both $g(r)$ and $u(r)$ can be used to calculate important equilibrium thermodynamic quantities, such as, the potential energy

$$U = \frac{N}{2} 4\pi\rho \int_0^\infty r^2 u(r) g(r) dr \qquad (3a)$$

the macroscopic pressure,

$$P = \rho k_\beta T - \frac{2}{3}\pi\rho^2 \int_0^\infty r^3 \frac{du(r)}{dr} g(r) dr \qquad (3b)$$

(k_β being Boltzmann's constant), and the isothermal compressibility ($\kappa_T = -V^{-1} (\partial V/\partial P)_{T,N}$) [27,30,31]. Such relations are of particular value for non-crystalline systems like liquids, solutions, dense gases and amorphous solids, for which alternative methods are limited. Note, however, that the results will not be as accurate as directly calculating these properties because of the averaging involved in the calculation of $g(r)$. The usability of RDFs in determining structural parameters, like the structural coordination number z and its changes with physical transformations of the system, has been extensively demonstrated[24,32].

For crystals the RDF approach provides a series of delta functions along any crystallographic direction. The radial distribution function of a liquid is intermediate between the gas and the solid (Fig. 4), with a small number of peaks at short distances, superimposed on a steady decay to a constant value at longer distances (dilute gas pattern, see Fig. 4a). The presence of a peak indicates a particularly favored reparation distance for the neighbors of a given particle, thus providing valuable structural information. In the solid state, maxima and minima appear with positions explained in terms of coordination shells of particles packed around the central reference particle (Fig. 4c). The presence of an atom at the origin of coordinates excludes other particles from all distances smaller than the radius of the first coordination

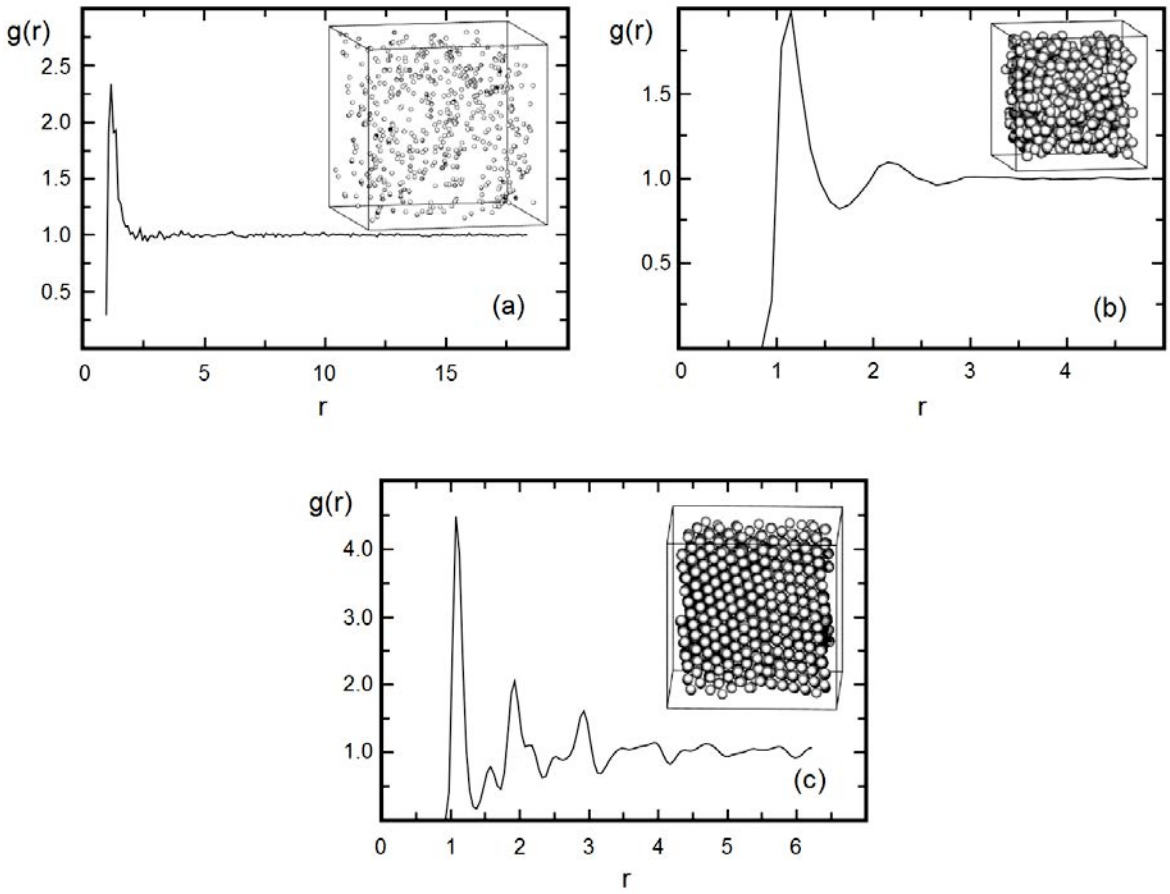

Figure 4. Example $g(r)$ plots of MD simulated (a) 500 particle Mie (Lennard-Jones) gas (number density = 0.01 and temperature = 1.0), (b) 500 particle Mie liquid (0.5 and 1.0, respectively), and (c) a 2000 particle Mie crystal (1.0 and 0.5, respectively).
Adapted from: *http://matdl.org/matdlwiki/index.php/softmatter:Radial_Distribution_Function.*

shell, where $g(r)$ has a maximum. It is worth noting that structural alterations –as measured by traditional static binary correlation functions – appear insignificant in the tempera-ture range of the glass transition phenomenon. Nevertheless, for reasons just stated, the RDF is still useful for describing some points of structure as well as for calculating certain properties of materials in the liquid and glassy states.

VORONOI POLYHEDRA FOR SPATIAL DESCRIPTION OF NONCRYSTALLINE SYSTEMS

In 1908 and 1909 a Ukrainian mathematician, Hrihory Voronoi, published his two papers[33,34] defining a mathematical construct –together with its dual the Delaunay tessellation– essential for our understanding of the structure of amorphous materials. Before examining in detail the method of applying Voronoi polyhedra to amorphous systems, it is instructive to describe the scope of this approach. The partition of space into Voronoi polyhedra and analysis of their topological features and metric properties has numerous applications in local structure characterizations of disordered systems. The kinds of systems studied with the aid of Voronoi polyhedra include: hard-[35,36] or soft-sphere glasses[23,37]; liquid metals[25,26]; molten[38] and hydrated[39] salts; nanoporous inorganic membranes[40]; water at ambient conditions[41], in super cooled[42,43] and stretched states[42], as well as at the vicinity of the critical point[43]; and other hydrogen bonding liquids[44].

Polycrystalline microstructures in metallic alloys are commonly represented using Voronoi tessellations[45,46]. However, the use of the Voronoi method is not limited to the field of condensed matter physics but finds applications from biophysics[47], biology, and physiology to astrophysics[48] (e.g. fragmentation of celestial bodies, for instance, to describe quantitatively results of a collision of two meteorites), bioinformatics[49] and mathematics[50]. Since Voronoi cells can be defined by measuring distances to areas as well as to points, the approach is being used in image segmentation, city planning, optical character recognition and other applications[51].

Now more to the subject at hand, the glassy state: macromolecular systems are often found in the glassy state, since irregular chain architecture may inhibit crystallization under typical polymerization conditions, under compression of as-received amorphous specimens, or even under very slow cooling of their melts. Consequently, applications of Voronoi-Delaunay structural analysis to polymer science have appeared at an increasing rate, with important results extracted for simple linear-chain polymers[52-59], as well as for grafted polymers[60], polymeric foams[61], dense colloidal suspensions[62] and biopolymers (proteins, lipid membranes, etc.)[63,64].

The starting point for the description of polymer structure is the concept of densely packed, entangled, random Gaussian coils[65], a notion derived from studies on polymer solutions and melts. Like inorganic glasses and glass-forming liquids, the structure of an amorphous polymer exists in a metastable state with respect to its crystalline form (although in certain circumstances, for example in atactic polymers, there is no crystalline analogue of the amorphous phase). Therefore, experimental and theoretical approaches dealing with the short-range dynamics of microstructural elements and with the spatial description of polymers are crucial in our attempt to provide interpretations of these phenomena on the microscopic level. In the next section, a description of the Voronoi-Delaunay method is provided. Selected applications will be discussed, with emphasis on structural descriptions and local particle-dynamics studies of macromolecular substances and composites (so-called polymer-based materials or PBMs). Our focus on this particular class of amorphous materials is dictated by their expanding usage as metal part substitutes in, e.g., automotive and aeronautics industries and other engineering applications[66,67].

THE VORONOI-DELAUNAY APPROACH

If one were to investigate zirconia ceramics, one could not adequately do so without a working knowledge of Miller indices since that knowledge makes it easy to understand and explain the structures and behaviors of the crystalline material. As new tools to describe amorphous materials are developed, it likewise behooves one who works with non-crystalline materials to acquire knowledge of those techniques. Therefore we shall explain in some detail how to use Voronoi polyhedra and their mathematical dual, Delaunay simplices, to better define and describe glassy materials.

A Voronoi polyhedron is defined as the (usually) convex region of space closer to its central particle than to any other. It is constructed – according to a unique mathematical procedure – for individual physical entities, hereafter called *particles* (e.g., ions, atoms, radicals, molecules or polymer chain segments)[3,52,68,69]. In this procedure, each particle is principally characterized by the location of its geometrical center and by the size and shape of the surrounding polyhedron. For a set of points on a flat surface (2D space), with each point representing a particle, links are drawn between neighboring points (the so-called Delaunay triangulation process). Then, for each link a line is drawn perpendicular to it and passing through a point equidistant from the terminal points. By removing the Delaunay triangulation, the bisectors produce polygons around the particles. For each particle, the smallest polygon so constructed is the Voronoi polygon; the sum of all polygons constitutes the

Voronoi diagram (illustrated in Figure 5).

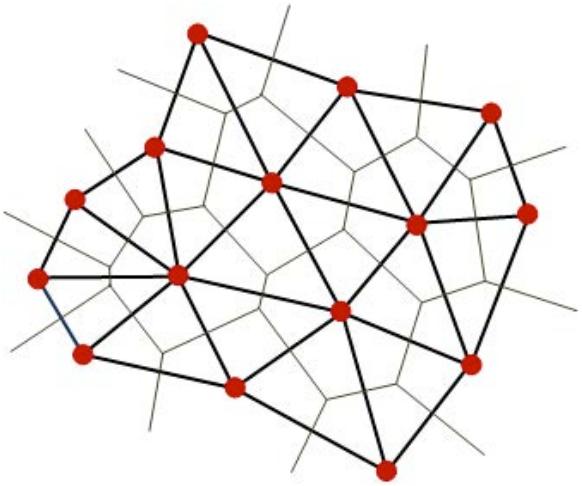

Figure 5. Delaunay diagram (thick lines) and Voronoi diagram (thin lines) for a given group of particles –represented by dots– in 2D space.

Extending the above construction to 3D, with bisectors as planes instead of lines, is straightforward. A quadruplet of geometrical neighbors (i.e. particles whose Voronoi polyhedra meet at a common vertex) forms another basic topological object called a Delaunay simplex; the four particles are called a simplicial configuration. One used to working with crystalline materials could easily apply the same approach to a simple 2D square lattice. The crystals are represented by Voronoi polyhedra, in this case squares (cubes in 3D). The Delaunay simplices are identical squares only shifted diagonally and equal to unit cells. This application of the Voronoi-Delaunay method to a square crystal lattice provides a simple illustration of the duality between Voronoi and Delaunay tessellations.

The procedure for constructing Voronoi polyhedra and Delaunay simplices in 3D is illustrated in Figure 6. The topological difference between these objects is that the Voronoi polyhedron represents the environment of individual particles whereas the Delaunay simplex represents the ensemble of neighboring particles (for conceptualization of this, consider again comparison to the crystal lattice). Furthermore, whereas the Voronoi polyhedra may differ topologically (i.e., they may have different numbers of faces and edges), the Delaunay simplices are always topologically equivalent. In three-dimensional space, two prevailing configuration types have been found based on several models of solids and monoatomic liquids: Delaunay simplices close in form to a regular tetrahedron ("good" tetrahedra) or to a quarter of a regular octahedron (quatroctahedra)[70]. The partitioning of space attained in the way just outlined constitutes the Voronoi tessellation process. When periodicity in local arrangement reaches long-range order the above process becomes identical to the Wigner-Seitz unit cell method for crystalline solids[4,71] and the construction of the first Brillouin zone (although the fcc Brillouin zone leads to a bcc Voronoi polyhedron, and vice-versa).

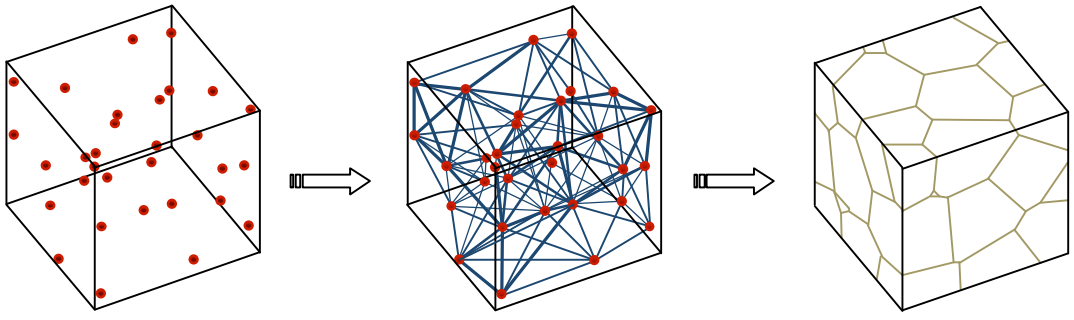

(a) Irregular point set (b) Delaunay tessellation (c) Voronoi tessellation

Figure 6. Partitioning of 3D space (a cube in the present case) containing a randomly placed set of particles (dots) into Voronoi polyhedra.

Since the shape of the Voronoi polyhedra and the arrangement of the Delaunay tetrahedra provide a measure of the local environment and of particle packing in amorphous systems, several topological characteristics and metric properties are in use. For each constructed polyhedron, Euler's formula[72]

$$N_\upsilon - N_e + N_f = 2 \quad (4a)$$

connects the number of vertices (N_υ), edges (N_e) and faces (N_f). In addition, since each vertex is the intersection of exactly three faces, and hence that of exactly three edges, whereas each edge connects exactly two vertices, it follows that

$$2N_e = 3N_\upsilon. \quad (4b)$$

N_f provides information on the number of geometric neighbors of the central particle, while the area of a face is related to the distance of the corresponding neighbor (i.e., closer neighbors generally share larger polyhedral faces). Voronoi polyhedra[23,37,54] are commonly measured by their volume (V_p), total surface area (A), shape factor (η'),

$$\eta' = \frac{1}{36\pi}\frac{A^3}{V_p^2} \quad (5a)$$

and curvature (C)

$$C = \frac{A}{24\pi V_p}\sum_i l_i\theta_i \quad (5b)$$

where l_i is the length of edge i of the polyhedron and θ_i is the angle between the normals of the intersecting faces[37,54]. The reciprocal of the Voronoi polyhedron volume characterizes the local density around the particle. By definition η' is 1 for a sphere and increases with increasing deviation from a spherical shape (e.g., it equals 1.33, 1.35 and 1.91 for a truncated octahedron, a rhombic dodecahedron and a cube, respectively). For the Delaunay simplex, descriptions include the tetrahedricity (Γ),

$$\Gamma = \sum_{i>j}(l_i - l_j)^2 / 15 l_{AV}^2 \quad (5c)$$

(where l_i is the length of the i-th simplex edge and l_{AV} is the average edge value for the simplex), along with octahedricity (O), perfectness (S), and void size (υ_T), i.e., the largest void that can be inscribed inside the tetrahedron without overlapping the particles[3,23,25,35].

By analyzing metric properties – such as the number of faces, polyhedron shape and volume, and related distributions – of an assembly of Voronoi polyhedra it becomes possible to appraise important phenomena and properties of non-crystalline materials. Notably these include the ability to monitor changes in the local structure and the free volume distribution as the collection of particles passes – with decreasing temperature – from the liquid or rubbery to the glassy state (glass transition phenomenon), and the possibility to describe percolative problems (e.g., phase transitions, and thermal or electrical conductivity percolation thresholds in polymer nano-composites). The 3D Voronoi tessellation method is now a well-established tool for geometrical description of the structure of amorphous polymers from sub-nano to macro-scale levels. Construction of Voronoi diagrams is a non-trivial problem for which a few algorithms have been proposed with variable success[23,36,69,73,74]; a related routine has been offered with MatLab 6.5™ (by The Mathworks Inc.), as well as with Materials Studio[75] and other software packages (e.g., the VORONOI program, provided by CAPCPO and running within AutoCAD™).

FREE VOLUME CONSIDERATIONS IN AMORPHOUS MATERIALS

We have made already a brief reference to free volume; and no discussion of structure as we are attempting at present can be complete without further explication of this important aspect. Within the macroscopic volume of a material, the so-called "*free volume*" v^f constitutes an equilibrium property of the system at temperatures exceeding T_g. The free volume is of paramount importance in relation to thermomechanical characteristics and engineering applications of most glassy materials, especially of polymer-based materials. Molecular motions in the bulk state

of polymeric materials are considered to depend on the presence of structural voids, also known as "vacancies" or "holes" of molecular size (typical hole volumes of 0.02-0.07 nm^3), or imperfections in the packing order of molecules. These holes are collectively described as free volume, a term also used to describe the excess volume that can be redistributed freely without energy change. At sufficiently fast cooling rates from the rubbery state to $T < T_g$, the spatial position of chains, with their folds and constraints, remains fixed and unrelaxed to a large extent. Part of the unoccupied free volume spontaneously perishes with a concomitant reduction of both the bulk volume and the equilibrium end-to-end distance of chains. The residual v^f strongly depends on the starting temperature of the quenching process, the cooling rate, and the conformational characteristics of the polymer chain.

Quantitative determination of free volume is performed infrequently, and that despite the fact that several well-established methods exist. For example, in glass-forming liquids, molecular simulations are used to examine changes of local structure and free volume in the temperature region approaching the glass transition. For probing pore sizes, pore size distributions and pore connectivities of polymeric systems, techniques including positron annihilation lifetime spectroscopy (PALS), computer modeling, and numerical analyses of amorphous cells have been extensively implemented[54,76]. Moreover, computer simulations provide equilibrated polymer configurations which permit Voronoi tessellations of structural groups (atoms, compounds, monomers, chains, etc.) to be constructed and also examined along the macromolecular chain; density fluctuations, ranging from very narrow[54] to very wide[52], and anisotropic distribution of free volume[53,56] have become evident in that way. Additionally, through computer simulations collections of particles can be classified into liquid- or solid-like categories on the basis of free volume and on the basis of shape and distortion of the Voronoi polyhedra and Delaunay simplices[23,37,77]. When described in such a geometric way, the unoccupied volume is no longer treated as a "hole" or "free" volume, but rather it is associated with the immediate environment of individual groups (e.g. side-chains) and the topology of the chains. Therefore it will change as the polymer is heated, deformed[78], or mixed with another material (e.g., in the form of miscible binary polymer or oligomeric organic + polymer blends[80-82]). It should be noted, however, that the Voronoi polyhedron volume only gives an indication of the volume available in the periphery of a particle; quantitative free-volume estimates necessitate subtraction from the polyhedron volume of the hard-core volume of the particle enclosed (i.e., the incompressible volume occupied by the particle at absolute zero temperature and an infinitely high pressure).

Several reports highlight the importance of the notion of the distribution of free volume, rather than that of the total free volume of a material. Free volume distribution contributes significantly to several thermal, mechanical and rheological properties of a polymer system. Its evolution in the course of different time-dependent thermomechanical and physico-chemical treatments (drawing or stretching deformation, physical aging, curing, etc.) is a matter of interest for material scientists and engineers. Details of the fine structure of amorphous systems can be derived by considering individual "atomic" polyhedra. When such systems are analyzed in terms of Voronoi polyhedra they show wide variations in packing density on the atomic/monomer scale, with a characteristic skewed distribution; in fact, the width of the monomer Voronoi volume distribution is regarded as a measure of amorphicity.

The combined molecular dynamics and Voronoi tessellation analysis of amorphous poly(trimethyl terephtalate) (PTT)[55], a model linear polymer resembling polyethylene[53], and of other types of unentangled linear chains[57,58], has successfully addressed the applicability of the Voronoi approach in free volume distribution determinations. It is worth noticing that atomistic simulation studies of "simple"

linear polymer chains are rather common, since such systems encompass the essential attributes of connectivity, constrained flexibility and van der Waals interactions. Jang and Jo[55], for example, analyzed chain conformation characteristics, such as bond orientation, the dihedral angle, and Voronoi volume tessellation, and showed that the PTT chain under extension undergoes conformational changes different from those under compression. Voronoi volume distribution was found to broaden with strain under extension and shrivel under compression, with a concomitant decrease in free volume. Stachurski[52,82] provided another illustrative example of this behavior through a computer simulation study of a cell of poly(methyl methacrylate) (PMMA), comprising 9000 atoms. The analysis of such virtual amorphous cells revealed large periodic density fluctuations, which in uncrosslinked polymers led to – and provided evidence for – the concept of constriction points; at locations along the chain where the local Voronoi volume is minimal, the surrounding atoms act as constrictions on the molecular chain within[52,78].

The free volume distribution in polymer systems is expected to be influenced by tacticity and side group substitution. By comparing pore distributions obtained from PALS measurements with the static free volume distribution obtained from amorphous cells simulated using the Voronoi tessellation of space, Dammert, et al.[83] have explored these features using poly(p-methyl styrene) and polystyrene as model systems. The results indicated broader hole distributions for the syndiotactic specimens compared to the more atactic samples. On the other hand, modeling revealed that the methyl substituent broadens the distribution of free volumes considerably; a behavior documented in the positron annihilation results as longer lifetimes and larger volumes of the holes. The maxima in the free volume hole size distribution were of smaller values for the polystyrenes than for the poly(*p*-methyl styrene)s. Interestingly, calculations also revealed the presence of a large number of undersized holes (due to the spacing among functional groups in the polymers), with dimensions outside the PALS measuring sensitivity.

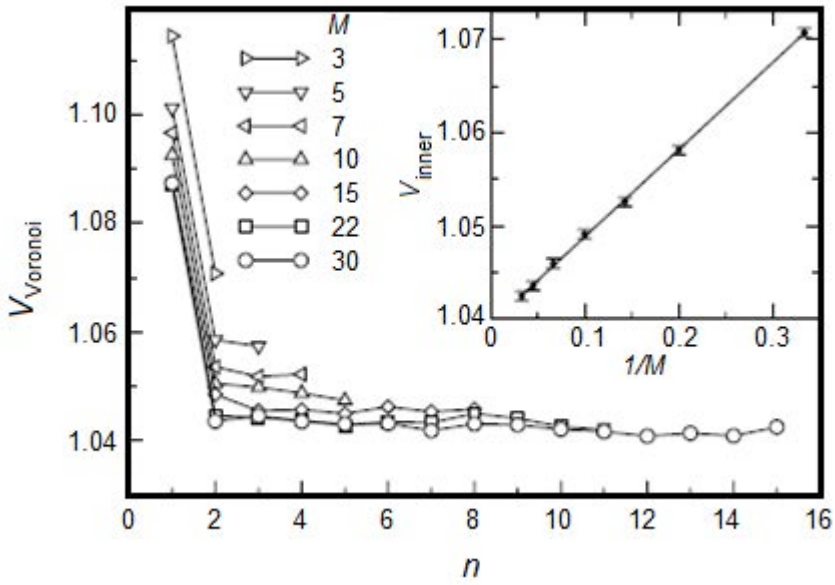

Figure 7. Average volume of the Voronoi polyhedron around the particle located at the *n* position along the chain (symmetric positions with respect to the centre of the chain are averaged over *n*, with $n \leq M/2$, M = chain length). Note the larger volume of the polyhedra surrounding the chain ends ($n = 1$). Inset: chain length dependence of the Voronoi volume of the inner polyhedra (from Ref. 57).

The chain length dependence of the glass transition temperature in polymers is often explained by the higher free volume surrounding chain ends[57,76,84]. The Voronoi polyhedron volume associated with a chain end has been reported to exceed the average Voronoi volume[57,59,76] (Figure 7). Similar arguments apply to both non-deformed structures and model systems experiencing extensional strain[53]. For polymers with either flexible chains or strong intermolecular interactions, the nucleation of cavities upon deformation occurs preferentially near the chain ends[58]. Simulations results of the effect of stretch and the resulting molecular orientation on the free volume distribution in a poly-ethylene-type polymer confirmed the exper-imental observation that chain alignment (due to increasing extensional strains) causes a decrease both in the total number of voids and the number-average void size. At the same time there is an increase in the number of larger, more elliptical empty cavities (voids) in the polymer[85] due to the extensional strain. The effective density increases as result of a decrease in the total free volume but it is not distributed evenly; free volume associated with atoms located away from the ends (i.e., atoms generating the so-called "inner" polyhedra) decreases, while the free volume associated with atoms located at the molecular ends increases with stretch. In a recent simulation study of the nucleation and growth of voids (cavitation process) that precedes craze formation, and the early crazing itself, occurring in rod-containing polymer nano-composites, it was found that the Voronoi volume can anticipate void formation and that it can also be used as a predictor of failure, particularly in composite materials[86].

The free volume is important to understanding the glassy state especially as it applies to relaxation dynamics – and we may recall from section 3 the significance of relaxation times in our characterization of glasses. Here we expand the discussion to include relationships with chain structure and v^f. The Voronoi space division of topologically different groups has been explored[60] through MD simulations of a 500-mer polyethylene model chain linked by 50 hexyl groups as side-chains (i.e., a grafted polymer having 52 ends). End (CH_3–), internal (–CH_2–), and junction (>CH–) groups exhibit different Voronoi polyhedra shapes with volumes decreasing by group in the same order as they are here mentioned (Fig. 8). Chain-end volumes are the most sensitive to temperature, indicating higher mobility for these units. Moreover, chain ends dominantly localize at the material's surface. This striking result involved the observation that while the ratio of surface groups was only 24% of all atoms, the ratio of ends at the surface was 91% out of all ends. This "preference" has direct consequences in the interpretation of accelerated relaxation dynamics, namely that as the surface is approached, we observe a gradual change along with increasing relaxation frequencies. Furthermore there is a concomitant depression of the global glass transition temperature reported for polymers in the form of free-standing or supported (on to repulsive surfaces) ultrathin films[87]. Therefore we infer a significant relationship between chain topology, free volume, and the glass transition temperature. Such connections are just beginning to be fully appreciated and utilized in research pertaining to the glassy state.

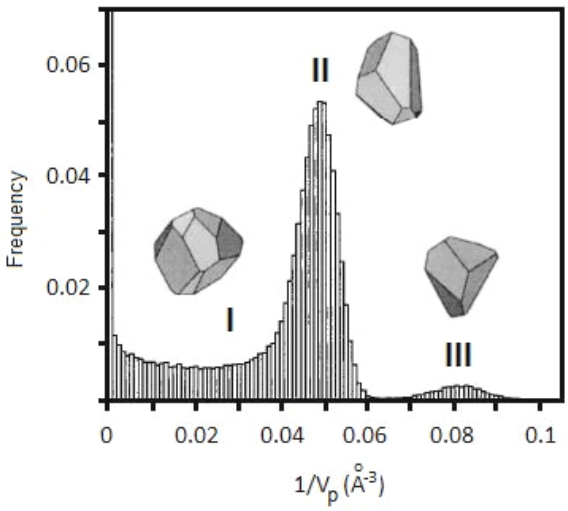

Figure 8. Histogram of the frequency distribution of the inverse polyhedron volume $1/V_p$ at 300 K for various groups. The exceptional peak at $1/V_p = 0$ corresponds to open polyhedra. I indicates a small shoulder near $1/V_p = 0.03$ (*end* groups), the Gaussian-type peak II at $1/V_p = 0.05$ corresponds to *internal* groups, and peak III near $1/V_p = 0.08$ corresponds to *junction* groups. The Voronoi polyhedra of the three types of centers are also shown.[60]

LOCAL STRUCTURE, GLASS DYNAMICS AND THE GLASS TRANSITION

We are now equipped to examine in further detail the local structure — as described by Voronoi polyhedra — of amorphous PBMs and the relationship to glass dynamics and the glass transition. A promising use of Voronoi networks involves its application to percolation analysis of amorphous structures. Using Voronoi networks, one can study diffusion and percolation properties of complex systems. Percolation theory is commonly used to describe natural phenomena that feature a continuous phase transition. For a given network, finding the critical point p_c (i.e., a probability, mass or volume fraction) at which the percolation transition occurs is a problem of particular interest. The glass-to-rubber or glass-to-liquid transitions in amorphous organic or inorganic systems as well as the conductor-to-insulator transition in insulating organic matrices with conductive inclusions constitute important percolative problems. There exist already examples of how Voronoi-type cells can be used for modeling thermal[88] and electrical[89-91] conductivities of various polymer nanocomposites. Gerhardt and coworkers[90,92], for example, describe for compression molded polymer-matrix composites the formation of a separated network microstructure in which the originally circular-shaped matrix particles reach polyhedral shapes upon compression. Specifically, for polymethyl methacrylate (PMMA)/carbon black (CB)[89], acrylonitrile butadiene styrene (ABS)/CB[91], and PMMA/indium tin oxide (ITO) nanocomposites[90], the polymer phases were roughly equivalent to ordered Voronoi cells (i.e., truncated tetrahedra, with 8 faces and 18 edges) in the microstructure with the filler nanoparticles aggregating along the edges of the polyhedra, thereby forming a structure comparable to nanowires (illustrated in Figure 9). Through this approximation it was made possible to interrelate the radii of the initially spherical matrix particle and filler (r_p and r_f, respectively) with the edge lengths of the deformed matrix particle and filler (a_p and a_f,

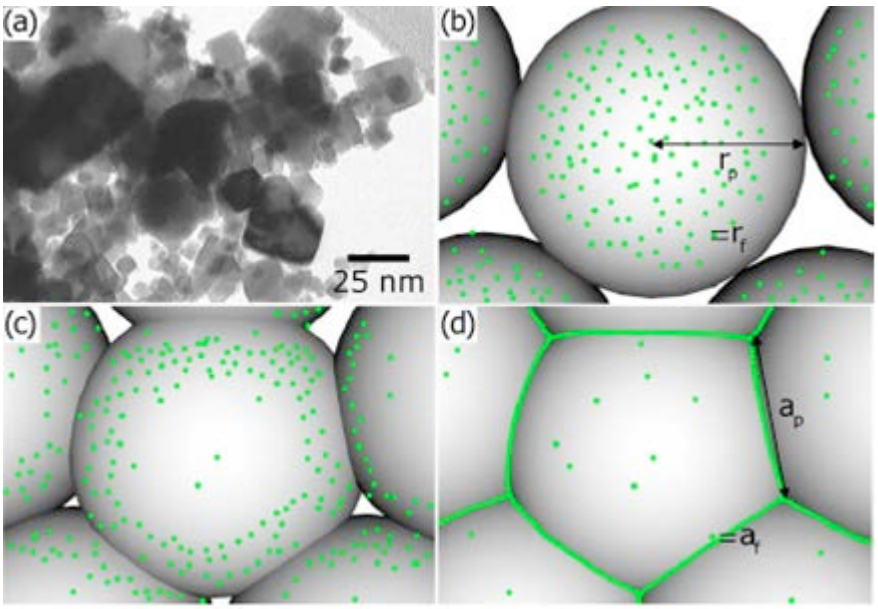

Figure 9. (a) Transmission electron microscopy (TEM) image of ITO nanoparticles. Images in (b), (c) and (d) are illustrations of ITO-coated polymer-matrix particles where the filler is depicted as small particles and the matrix is depicted as large particles: (b) before compression molding, (c) during compression molding, and (d) after compression molding in the final composite with an ITO content near the percolation threshold.[90]

respectively), and finally obtain theoretical predictions for the critical volume fraction of the filler[90]. Self-assembled structures such as these are the driving force for extremely low percolation thresholds, phenomena observed through electrical impedance analysis of samples with varied filler content. Thus we have multiple instances where the measured properties of amorphous PBMs are described through Voronoi networks.

The information presented so far provides unambiguous evidence for the physical significance of some simplicial particle configurations. For instance, Voronoi polyhedra with large circumradii denote low density configurations, and *vice-versa*. Along these lines, the Voronoi-Delaunay technique has been utilized for studying subtle differences in the structure of liquid and solid (quenched) phases[70]. Structural signatures in the form of percolation thresholds of Delaunay networks[26,70] and increase in icosahedral ordering near T_g[93] have been observed in cases of simulated amorphous solids and simple liquids. Structural information has been extracted by studying the percolation thresholds of networks of Delaunay simplices of different "coloring", where each color denotes Delaunay sites of identical form (i.e., with identical metric properties). For example, in a case study of the molecular dynamics configurations of liquid, super cooled and quenched rubidium, Medvedev and coworkers[26] indicated that the Delaunay simplices develop macroscopic aggregates in the form of percolative clusters. In the liquid state, clusters result from low-density atomic configurations. These macroscopic structural organizations in the liquid state permit extensive motions, like those in shear flow. In contrast to the low-density atomic configurations of the liquid state, nearly tetrahedral high-density configurations contribute to cluster formation in the solid state. In the liquid state, the low-density cluster goes across the whole material; in the amorphous solid state, the high-density cluster percolates across the whole glass.

In spite of the several differences reported, there is generally a lack of signatures of the glass transition in the particle positions on the molecular level. To overcome this lack of markers, a number of studies have focused on relationships between local structures, characterized by Voronoi polyhedron volume, and local dynamics, characterized by particle displacements[62]. In an interesting study back in 1997, Jund and coworkers[94] executed an atomistic study –for a simulated 1000-particle system– of the mechanism of the glass transition, analyzing the volume and surface distributions of Voronoi polyhedra above and below the system's T_g. A saturation of the density fluctuations was verified as a signature of the transition in the system cooled from the liquid state. Moreover, evaluating deviations of the cell shapes from a regular dodecahedron, the authors observed that the fraction of non-pentagonal cell faces increases with temperature in the glassy phase, at the expense of 5-edged faces, while at the glass transition the trend is reversed and a majority of pentagons is recovered in the liquid state. Another research group[95,96] approached the glass transition phenomenon by distinguishing between "liquid-like" and "solid-like" defects: the concentration, c_ℓ, of liquid-like defects – defined by them as small particles enclosed in heptagons or octagons, and large particles enclosed in pentagons or even squares– was shown to nearly vanish in the glass state. A typical scale parameter was defined as $\xi \equiv \sqrt{c_\ell}$, and found to diverge at T_g[95], in a way analogous to the divergence of the relaxation time of a viscous fluid as temperature approaches T_g.

Gil Montoro and Abascal[23] performed microcanonical MD simulations of a model glass-sphere system featuring Mie (Lennard-Jones) interactions. This study revealed that both the width and asymmetry of the Voronoi volume distribution increases when going from the solid to the liquid and finally to the gas (i.e., a simulated non-interacting fluid) state (Fig. 10a). Furthermore, the nonsphericity α distribution ($\alpha = RA/3V_p$, R being the average

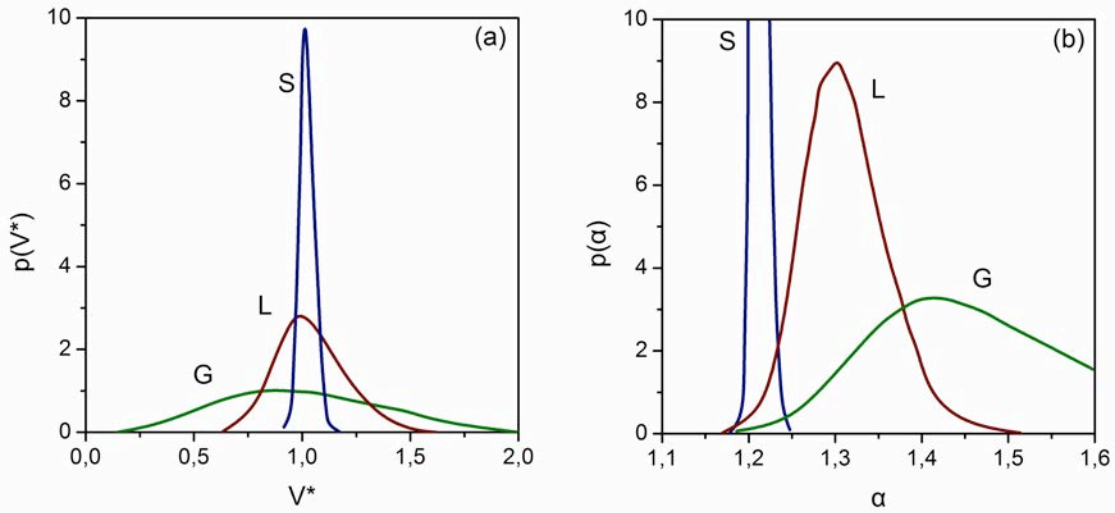

Figure 10. (a) Voronoi polyhedron volume distribution functions about the mean ($V^* = V_p/V_{p(mean)}$), and (b) nonsphericity (α) distribution functions, for simulated solid (S), liquid (G) and gas (G) systems. Replotted graphs from Ref. 23.

curvature radius of the convex body) demonstrated the highest versatility in describing structural differentiations among the three states (Fig. 10b).

Establishing connections between local structure characteristics and vibrational properties in glassy systems remains an open issue. A valuable theoretical framework in this pursuit is the potential energy landscape (PEL, mentioned earlier), where energy is partitioned into basins connected by saddle points—a system, which represents the complicated dependence of energy on configuration[97]. When studying dynamics in the glassy state one assumes a separation of time scales as the system approaches the glass transition temperature; short-time motions are considered to occur via intrabasin vibrations about a particular structure (a local potential energy minimum), while long-time motions take place via occasional activated jumps over saddle points into neighboring basins. In an amplification of this concept, the picture of "metabasins" has been introduced[98]. Each metabasin consists of several local minima separated by low energy barriers; the α-relaxation (the signature of the glass-transition process in dynamic experiments) occurs via jumps between neighboring metabasins, with molecular motions proceeding in a cooperative manner. Numerous applications of the PEL approach have been reported, including the establishment of links between its topography and the dynamics for binary Lennard-Jones glasses[97], and the identification of significant confinement-induced differences among model bulk and free-standing polymer films[99]. Jain and de Pablo[100] performed detailed computer simulations of a model super cooled polymer, near its apparent T_g, exploring the role of the local "inherent" structure of particles (i.e., of their Voronoi polyhedron) on motions on the PEL[101,102]. Their results indicated that the time of vibration of a particle in a metabasin correlates with the structure of its Voronoi polyhedron and with the number of its neighbors; the largest metabasins corresponded to particles whose average Voronoi volume was close to the value expected on the basis of the density, and whose approximate number of neighbors approached 12 (icosahedral ordering). The local distortion around a particle, measured in terms of the tetrahedricity of the Delaunay simplices, also revealed that particles with a higher degree of local distortion are likely to transition faster to a neighboring metabasin. The above arguments stress the significance of the identification of structural motifs in understanding the influence of chemical structure on the dynamics in glass formers.

On a totally different –yet still related– direction, Luchnikov and coworkers[37] studied atomic configurations in a simple soft-sphere model glass and demonstrated the usability of the Voronoi-Delaunay structural approach in deciphering correlations between normal-mode vibrations with parameters characterizing local-structure perfectness (i.e., *O*, *S* and *Γ*, defined above). In combination with a conventional harmonic vibrations analysis the conclusion drawn was that in real space the lowest-frequency quasi-localized vibrations can be envisaged as being caused by instabilities in local geometry.

VORONOI TOPOLOGIES OF MICROSCOPY IMAGES

A majority of theoretical studies based on statistical physics that incorporate the Voronoi-Delaunay approach analyze objects existing within virtual space created by a computer. Nevertheless, in the discipline of applied materials science geometric analyses of Voronoi topologies involve –on a more and more frequent basis– *real* structural information acquired, among other techniques, from scanning electron (SEM), atomic force (AFM) and scanning tunneling (STM) microscopy images[61,90,103-105]. Nearly two decades ago, Stange, et al.[105], using AFM and STM, followed the evolution of spin-coated polystyrene films on silicon surfaces from individual isolated molecules to a continuous film. At a critical polymer concentration in toluene (the polymer's solvent), they observed the formation of 2D Voronoi tessellation-like networks of polystyrene molecule aggregates, which they subsequently discussed in terms of a specific failure mechanism leading to film rupture in spin-coating processes. Recently, Song et al.[106] used Voronoi diagrams and bond-orientation correlation functions to analyze microscope images of "structured" microporous polymer films (i.e., films with closely packed hexagonal arrays of pores). A direct measurement of the open pore sizes and their distribution was made possible.

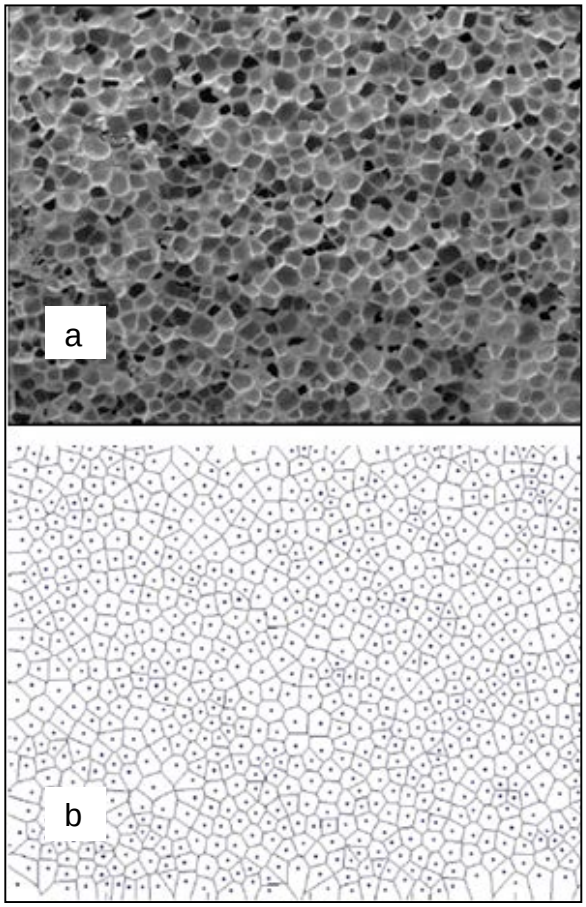

Figure 11. (a) SEM image of a polymeric foam (×100), and (b) its Voronoi diagram.[61]

Jacobs and coworkers[61] recently discussed a quantitative method for the comparative Voronoi analysis of various polymeric foam morphologies. At the foundation of their analytical technique are parameters related to the average Voronoi cell area, cell area distribution, and foam homogeneity. As a first step in this approach, cell walls are visualized with SEM analysis of a cross section of the foam (Fig. 11a). Using only the perimeter of the cells as markers, the cell structure appearing in such images is subsequently converted into a grid (using MatLab™) after which the Voronoi diagram is constructed (Fig. 11b). The homogeneity of the foams could thus be described in terms of cell area, perimeter and number of faces. Using poly(styrene-co-methyl methacrylate) foamed with supercritical carbon dioxide as model system, Jacobs et al.[61]

demonstrated the ability of the above method to reveal even slight changes in a foam's homogeneity. The accuracy of the constructed Voronoi diagrams is clearly dependent on the perspicuity of the SEM pictures; use of sufficient contrast between the voids and the continuous phase is mandatory.

Similar descriptors are applied to morphological characterizations of fiber reinforced composites in terms of Voronoi polygons[103,104]. For example, the transverse spatial distribution of glass fibers in continuous fiber reinforced epoxy microstructures has been described using Voronoi polygon areas and nearest neighbor distances as spatial descriptors[103]. In such an approach, Voronoi tessellations with fibers located at cell centers were generated from SEM micrographs. Convergence towards global distributions was observed (for both metric properties) at increasing sample sizes for most of the systems studied. Statistical tests provided estimates of the size of the volume element (i.e., a sampling area dimension), which is representative of the global microstructure and inhomogeneity in each material. At the scale of this "representative" volume element any sample taken of the actual composite structure is deemed equivalent, and representative, of the entire microstructure.

Concentrated colloidal suspensions are also of interest as they may exhibit a distinct glass transition whose value is a function of particle concentration or density. Using dense colloidal suspensions as a model system, Conrad and coworkers[62] searched for correlations among the Voronoi volume and particles' displacement. Particle positions were imaged by confocal microscopy using fluorescently labeled polymer spheres. Results indicated that the scaled (by the standard deviation) distribution of Voronoi volumes around the average Voronoi volume is universal for dispersions with a hard interparticle potential (i.e., super cooled liquids containing "hard spheres" with a Lennard-Jones type potential). The scaled distributions were shown to fall onto a universal curve over a wide range of volume fractions of the polymer spheres in the colloidal suspension, in excellent agreement with the simulation results.

GLASS TRANSITIONS IN BINARY SYSTEMS

Microstructure is a critical determinant of various thermophysical and mechanical properties of inorganic + organic composites and of miscible organic blends. Moreover microstructure is a key feature for materials in selected applications such as drug delivery systems and composite solid state dye laser matrices, among others. While the method of material processing makes some contribution to the resultant microstructure, that structure for organic polymer blends is also inherently dependent on the balancing among inter- and intra-molecular interactions and the ensuing local density fluctuations. Molecular packing is clearly reliant on chemical composition, polymer chains conformation and configuration, and the degree and relative strength of enthalpic and entropic factors. Given the complexity of the underlying mechanisms in such polymer systems, a usually inhomogeneously dispersed population of structural voids appears, with dimensions extending even up to ~10 nm. Connected to all these attributes of amorphous binary systems is the glass transition – and with it relationships to microstructure.

Microstructural peculiarities are evident in miscibility studies of binary polymer[79,80] and drug + polymer mixtures[81,107]. Notably, the glass transition temperature of these systems manifest anomalous dependencies on composition (φ, as a mass fraction) (Figs 12, 13). Even in cases of athermal binary mixtures, there is ample experimental evidence in binary mixtures that the thermodynamically predicted smooth and monotonic $T_g(\varphi)$ variation, confined within the transition temperature region of the constituents, is often violated. This is the case irrespective of the problems encountered in defining or locating the T_g of a given system – an issue also partly related to kinetic attributes of the glass transition.

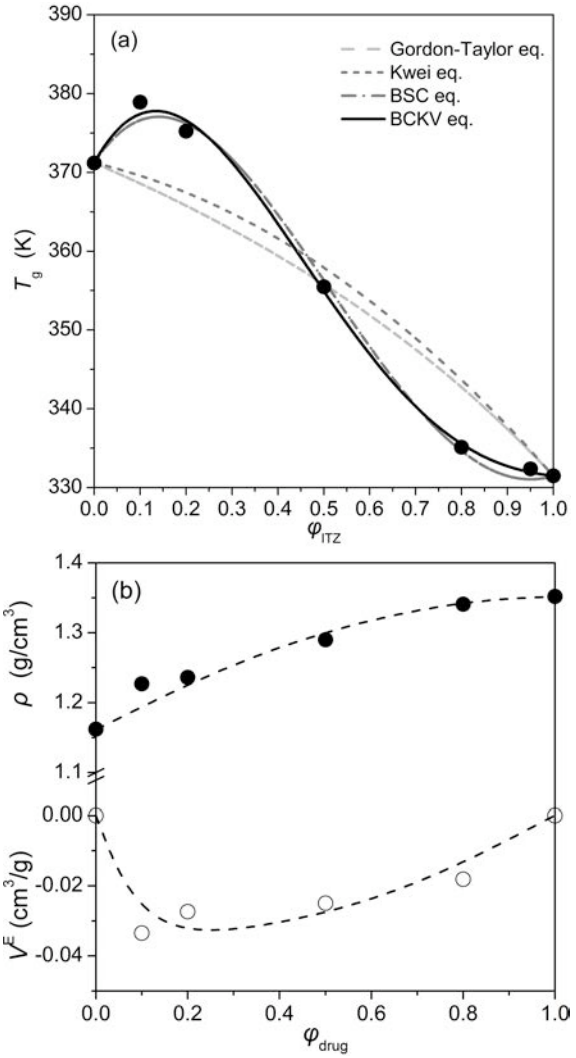

Figure 12. (a) T_g vs. composition dependence of Intraconazole (ITZ) + PLS-630 blends, and (b) compositional variation of density ρ and excess mixing volume V^E (per gram of mass) for the same mixture. Compiled from data appearing in Ref. 107.

Quantitative description of the deviations from ideality has been attempted through various theoretical and semi-empirical equations[81], with the most system-inclusive approach only very recently proposed (by Brostow, Chiu, Kalogeras and Vassilikou-Dova)[108] in the form of the function

$$T_g = \varphi_1 T_{g,1} + (1-\varphi_1)T_{g,2} + \\ + \varphi_1(1-\varphi_1)[a_0 + a_1(2\varphi_1 - 1) + a_2(2\varphi_1 - 1)^2] \quad (6)$$

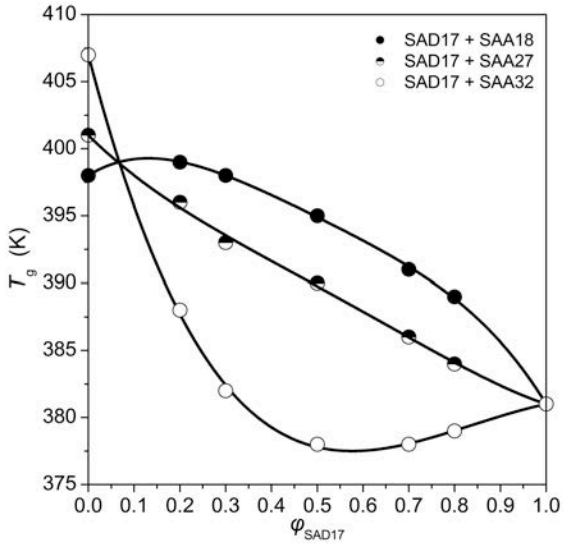

Figure 13. T_g vs. composition dependence of poly(styrene-*co*-N,N-dimethylacrylamide) [with 17 mol % of N,N-dimethylacrylamide] (SAD17) + poly(styrene-*co*-acrylic acid) [with 18, 27 or 32 mol % acrylic acid][80]. Thick lines are fits to the BCKV equation (6).

with φ_1 denoting the mass fraction of the low-T_g component. Eq. (6) is more recently called the BCKV equation[81]. The quadratic polynomial on its right side, centered around $2\varphi_1 - 1 = 0$, is defined to represent deviations from linearity. The type and level of deviation is primarily described by parameter a_0, which mainly reflects differences between the strength of hetero- (intercomponent) and homo- (intracomponent) interactions. The magnitude and sign of the higher-order parameters a_1 and a_2 is dictated by composition-dependent energetic contributions from hetero-contacts, entropic effects and structural heterogeneities (e.g., nanocrystalline phases). Along these lines, the number and magnitude of the parameters required to represent an experimental $T_g(\varphi)$ pattern provide quantitative measures of a system's complexity. Evidently, irregularly positive or negative –or even sigmoidal– deviations from the linear mixing rule are strongly linked to the compositional dependence of the total free volume and the free volume distribution around pertinent chain segments. All these "asymmetric" entropic or enthalpic contributions are expected to reflect

in the volumes and numbers of faces of the composite polyhedra of structural particles (e.g., monomers for polymers and molecular polyhedra for oligomeric organics).

Voronoi analysis of binary systems is in principle possible, e.g., by using MD simulations to obtain equilibrated structures[109,110] and developing appropriate analysis codes. For example, there was recently a report[109] of MD simulation of the compatibility of chitosan (CS) + poly(vinyl pyrrolidone) (PVP) biomedical mixtures. Although the Voronoi tessellation analysis was not conducted, the binary RDFs could be calculated from amorphous cells obtained for selected blend compositions. The RDF behavior (Figure 14) confirmed the supposition that the components' miscibility arose from hydrogen bond formation among the –C=O group of PVP and the $–CH_2OH$ group of CS. A Voronoi-Delaunay analysis of that particular mixture would be of high interest to our present discussion, especially given the strongly sigmoidal shape of its T_g vs. composition pattern[111] and its classification as a "high-complexity" binary system[81].

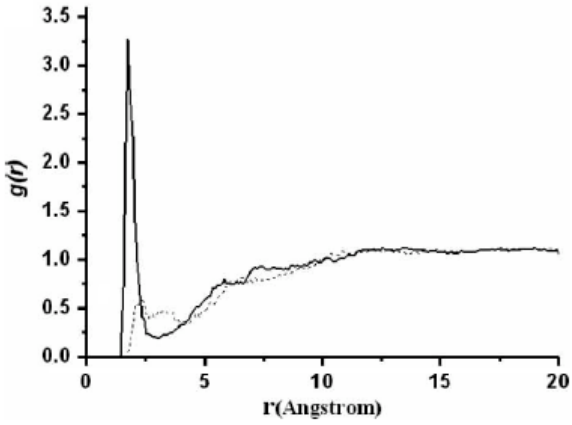

Figure 14. RDF calculation for a miscible 80/20 (molar fraction) CS + PVP blend, using the hydrogen atom of the hydroxyl methyl group of chitosan (solid line) and the hydrogen atom of the $–NH_2$ group of chitosan (dotted line) relative to the location of the oxygen atom of the carbonyl group of PVP[95].

Considering the increased depth and image resolution of contemporary microscopy apparatuses discussed in the previous section, one may attempt performing V-D analysis of electron miscoscopy images of miscible blends as spin casted or solvent evaporated thin films, for example. However, development of sufficient suitable codes remains an unsolved problem. Likewise, selection criteria are needed for distinguishing among the two different populations of "composite" polyhedra in a binary mixture; for example, the ones generated by drug molecules and those encompassing preselected polymer segments (i.e., the elementary unit of a monomer).

SUMMARY

Considerable literature exists regarding the representation of structures of amorphous materials. Of the available approaches, the Voronoi-Delaunay tesselation technique and the radial distribution function are usable for any material structure – crystals included. The experimental information and theoretical analyses discussed in this review exemplify their efficacy for quantitative local-geometry investigation[112] of various types of non-crystalline solids. In view of that, both approaches warrant inclusion in Materials Science Education (MSE) courses and should be taught along with the venerated crystallographic methodology.

A brief scheme of an introductory MSE module, or a pertinent educational presentation that makes use of the information previously presented, is given in Table 1. Several computational-geometry routines and applets are available[113-119] for instructors interested in an attention-grabbing interactive demonstration of the construction of Voronoi diagrams and Delaunay triangulations in any random set of particles. Representative tools proffer the Java™ applets of Paul Chew[114] (Cornell University), Andreas Pollak[115] or Christian Raskob[116] (University of Hagen), which were created as part of their diploma dissertations or

related activities. The VoroGlide applet[117] (University of Hagen) is another interesting program for interactive Voronoi diagrams, offering a single step animation mode for the incremental Delaunay construction and a recorder for teaching purposes. There are also a number of websites providing educational programs that can serve as sources of interest for the novice in the field. For example, a webpage under the title "Weighted Voronoi Diagrams in Biology" describes a program that constructs weighted Euclidean and power diagrams for computer simulation and analysis of a system of growing plants[120]. It also demonstrates application of power diagrams to problems from the fields of biology and ecology. Sites such as this, along with the mentioned applets, provide an opportunity for practical exercise of the concepts outlined in Table I and discussed in this review.

Table I. Proposed plan of an introductory MSE module, related to the Voronoi-Delaunay representation and analysis of non-crystalline structures and other applications.

Steps	**Visual tools (suggestions)**	**Training resources (Java™ applets, etc.)**
1. Introducing basic notions		
a) States of matter: Gas, Liquid, Solid.		
b) The solid state: Glasses vs. Crystals.	Fig. 1.	
c) Glasses vs. Liquids: The glass transition.	Fig. 1; Fig. 2; Fig. 3.	
2. Structure descriptors		
a) RDFs	Fig. 4 (and comparison with δ-function RDFs of typical crystals).	
b) The Voronoi-Delaunay (V-D) approach: Construction and metric properties.	Fig. 5; Fig. 6 (and comparison with crystallographic notions).	Real-time practicing with V-D graphs[113-118]
3. V-D analysis: *case studies*		
a) Free-volume distribution in polymers.	Fig. 7; Fig. 8.	
b) Local structure and transitions.	Fig. 9; Fig. 10.	
c) Polymeric foam morphologies.	Fig. 11.	
4. Ideas for future applications		
a) Modeling glass transitions in binary systems.	Fig. 12; Fig. 13; Fig. 14.	
b) and more, from instructor's research field…		Voronoi & biology[120] Voronoi & fractals[121,122]
5. Time for relaxation: *The Voronoi game!* [123] A two-player game based on a simple geometric model for the "competitive facility location". Competitive facility location studies the placement of sites by competing market players. The geometric concepts are combined with game theory arguments to study if there exists any winning strategy.		

ACKNOWLEDGEMENTS

This article is to some extent a byproduct of our research on thermoelectric materials supported by the II-VI Foundation, Bridgeville, PA. Thanks are due to Prof. W. Brostow (Univ. North Texas, USA) for critical reading of the manuscript and stimulating discussions on Voronoi-Delaunay analysis of glassy materials.

REFERENCES

1. J.V. Yakhmi, *J. Mater. Ed.* **33**, 149 (2011).
2. J.R. Telle, and N.A. Pearlstime (eds), *Amorphous Materials: Research, Technology and Applications*, Nova Science, pp. 1-335 (2009).
3. W. Brostow, and V.M. Castaño, *J. Mater. Ed.* **21**, 297 (1999).
4. R.J.D. Tilley, *Crystals and Crystal Structures*, Wiley, Chichester, UK (2006).
5. M. Matsuo, *J. Mater. Ed.* **33**, 213 (2011).
6. Y. Waseda, E. Matsubara, and K. Shinoda (eds.), *X-Ray Diffraction Crystallography: Introduction, Examples and Solved Problems*, Springer, pp. 1-310 (2011).
7. P. Ehrenfest, P. K. Akad. Wet-Amsterd. **36**, 153 (1933).
8. E. Riande, R. Díaz-Galleja, M.G. Prolongo, R.M. Masegosa, and C. Salom, *Polymer Viscoelasticity*, Marcel Dekker, New York, USA (2000).
9. J.D. Menczel, and R.B. Prime, (Eds) *Thermal Analysis of Polymers, Fundamentals and Applications*, Wiley, Hoboken, New Jersey, pp. 1-688 (2009).
10. A.J. Kovacs, *J. Polymer Sci.* **30**, 131 (1958).
11. R.G. Beaman, *J. Polymer Sci.* **9**, 470 (1952).
12. L.E. Nielsen and R.F. Landel, *Mechanical properties of polymers and composites*, 2nd edn., Marcel Dekker, New York – Basel – Hong Kong (1994).
13. D. Chandler, *Introduction to Modern Statistical Physics*, Oxford University Press (1987).
14. H. Vogel, *Phys. Z.* **22**, 645 (1921).
15. G. Tammann, and W. Hesse, *Z. Anorg. All. Chem.* **156**, 245 (1926); G.S. Fulcher, *J. Am. Ceram. Soc.* **8**, 339, 789 (1925).
16. P.G. Debenedetti and F.H. Stillinger, *Nature* **410**, 259-267 (2001).
17. T. Hecksher, A.I. Nielsen, N. Boye Olsen and J.C. Dyre, *Nature Physics* **4**, 737-741 (2008).
18. C.A. Angell, *J. Non-Cryst. Solids* **131-133**, 13-31 (1991); C.A. Angell, *J. Non-Cryst. Solids* **354**, 4703-4712 (2008).
19. J.L. Green, K. Ito, K. Xu, and C.A. Angell, *Phys. Chem. B* **103**, 3991-3996 (1999).
20. C.A. Angell, *Strong and Fragile Liquids*, in: *Relaxations in Complex Systems* (Eds K.L. Ngai, and G.B. Wright) National Technical Information Service, U.S. Department of Commerce, Springfield, VA 22161, pp. 3-11 (1985).
21. C.A. Angell. *Heat Capacity and Entropy Functions in Strong and Fragile Glass-Formers, Relative to Those of Disordering Crystalline Materials,* in: *Glassy, Amorphous and Nano-Crystalline Materials: Thermal Physics, Analysis, Structure and Properties*, Volume 8 in the *Hot Topics in Thermal Analysis and Calorimetry series*, Šesták, Jaroslav; Mareš, Jiří J.; Hubík, Pavel (volume eds.), J. Simon (series ed.), **8**, pp. 21-40 (2011).
22. G. Adam, and J.H. Gibbs, *J. Chem. Phys.* **43**, 139-146 (1965).
23. J.C. Gil Montoro and J.L.F. Abascal, *J. Phys. Chem.* **97**, 4211 (1993).
24. W. Brostow, *Chem. Phys. Lett.* 49, 285 (1977).
25. W. Brostow, M. Chybicki, R. Laskowski and J. Rybicki, *Phys. Rev. B* **57**, 13448 (1998).

26. N.N. Medvedev, A. Geiger and W. Brostow, *J. Chem. Phys.* **93**, 8337 (1990).
27. J.-P. Hansen and I.R. McDonald, *Theory of simple liquids*, 3rd Ed., Academic Press (2006).
28. C.N.J. Wagner, *J. Non-Cryst. Solids* **31**, 1 (1978).
29. J. Crocker, *J. Colloid Interface Sci.* **179**, 298 (1996).
30. D. Frenkel and B. Smit, *Understanding Molecular Simulation: from Algorithms to Applications*, Academic Press (2002).
31. D.A. McQuarrie, *Statistical Mechanics*, University Science Books (2000).
32. E.M. Moroz, V.P. Pakharukova and A.N. Shmakov, *Nucl. Instr. Methods Phys. Res. A* **603**, 99 (2009).
33. G. Voronoi, *J Reine Angew. Math.* **133**, 97-178 (1908).
34. G. Voronoi, *J Reine Angew. Math.* **136**, 67 (1909).
35. A.V. Anikeenko and N.N. Medvedev, *J. Struct. Chem.* **50**, 761 (2009).
36. J.L. Finney, *Proc. R. Soc. London* **A319**, 479 (1970).
37. V.A. Luchnikov, N.N. Medvedev, Y.I. Naberukin and H.R. Schober, *Phys. Rev. B* **62**, 3181 (2000).
38. L. Pusztai, A. Baranyai and I. Ruff, *J. Phys. C* **21**, 3687 (1988).
39. J.C. Gil Montoro, F. Bresme and J.L.F. Abascal, *J. Chem. Phys.* **101**, 10892 (1994).
40. N. Rajabbeigi, B. Elyassi, T.T. Tsotsis and M. Sahimi, *J. Membrane Sci.* **335**, 5 (2009).
41. Y. Yeh and C.Y. Mou, *J. Phys. Chem. B* **103**, 3699 (1999).
42. G. Ruocco, M. Sampoli, A. Torcini and R. Vallauri, *J. Chem. Phys.* **99**, 8095 (1993).
43. R.D. Mountain, *J. Chem. Phys.* **110**, 2109 (1999).
44. P. Jedlovszky, *J. Chem. Phys.* **113**, 9113 (2000).
45. M.I. Mendelev, M.J. Kramer, R.T. Ott, *et al.*, *Phil. Mag.* **90**, 3795 (2010).
46. K.H. Kang, K.W. Park, J.C. Lee, E. Fleury, and B.J. Lee, *Acta Mater.* 59, 805 (2011).
47. A. Soyer, J. Chomilier, J.P. Mornon, R. Jullien and J.F. Sadoc, *Phys. Rev. Lett.* **85**, 3532 (2000).
48. T. Kiang, *Z. Astrophys.* **64**, 433 (1966).
49. J. Tsai and M. Gerstein, *Bioinformatics* **18**, 985 (2002).
50. N. Sukumar, B. Moran, A.Y. Semenov and V.V. Belikov, *Int. J. Nucl. Meth. Eng.* **50**, 1 (2001).
51. A.M. Becker and R.M. Ziff, *Phys. Rev. E* **80**, 041101 (2009).
52. Z.H. Stachurski, *Polymer* **44**, 6059 (2003).
53. H. Dong and K.I. Jacob, *Macromolecules* **36**, 8881 (2003).
54. M. Sega, P. Jedlovszky, N.N. Medvedev and R. Vallauri, *J. Chem. Phys.* **121**, 2422 (2004).
55. S.S. Jang, and W.H. Jo, *J. Chem. Phys.* **110**, 7524 (1999).
56. J. Blomqvist, B. Mannfors and L.-O. Pietilä, *Polymer* **43**, 4571 (2002).
57. A. Barbieri, D. Prevosto, M. Lucchesi and D. Leporini, *J. Phys.: Condens. Matter* **16**, 6609 (2004).
58. B. Sixou, *Molec. Simulat.* **33**, 965 (2007).
59. M. Canales, *Phys. Rev.* **E 79**, 051802 (2009); A. Makke, M. Perez, J. Rottler, O. Lame and J.L. Barrat, *Macromol. Theor. Simul.* **20**, 826-836 (2011).
60. N. Tokita, M. Hirabayashi, C. Azuma and T. Dotera, *J. Chem. Phys.* **120**, 496 (2004).
61. L.J.M. Jacobs, K.C.H. Danen, M.F. Kemmere and J.T.F. Keurentjes, *Comp. Mater. Sci.* **38**, 751 (2007).

62. J.C. Conrad, F.W. Starr and D.A. Weitz, *J. Phys. Chem. B* **109**, 21235 (2005).
63. P. Jedlovszky, N.N. Medvedev and M. Mezei, *J. Phys. Chem. B* **108**, 465 (2004).
64. C.W. David, *Biopolymers* **27**, 339 (1988).
65. P.J. Flory, *J. Macromol. Sci. B* **12**, 1 (1976).
66. G.L. Samuel and S.H. Yang, *Int. J. Adv. Manufact. Technol.* **26**, 819 (2005).
67. G.D. Rong, Y. Liu, W.P. Wang, X.T. Yin, X.F.D. Gu and X.H. Guo, *IEEE Trans. Visual. Comp. Graph.* **17**, 345 (2011).
68. G. Voronoi, *J Reine Angew. Math.* **134**, 198 (1908).
69. W. Brostow, J.-P. Dussault and B.L. Fox, *J. Comput. Phys.* **29**, 81 (1978).
70. Yu.I. Naberukhin, V.P. Voloshin and N.N. Medvedev, *Mol. Phys.* **73**, 919 (1991).
71. E.P. Wigner and F. Seitz, *Phys. Rev.* **43**, 804 (1933).
72. L. Euler, *Novi Comm. Acad. Sci. Imp. Petropol.* **4**, 109-160 (1752-1753).
73. M. Tanemura, T. Ogawa and N. Ogita, *J. Comput. Phys.* **51**, 191 (1983).
74. N.N. Medvedev, *J. Comput. Phys.* **67**, 223 (1986); M. Tanaka, *J. Phys. Soc. Jpn.* **55**, 3108 (1986).
75. D. Stoyan, W.S. Kendall and J. Mecke. in: *Stochastic geometry and its applications*, Wiley, Chichester, (1987).
76. D. Rigby and R.J. Roe, *Macromolecules* **23**, 5312 (1990); B.J. Sung and A. Yethiraj, *Phys. Rev. E* **81**, 031801 (2010).
77. Y. Hiwatari and T. Saito, *J. Chem. Phys.* **81**, 6044 (1984).
78. D.N. Theodorou and U.W. Suter, *Macromolecules* **19**, 379 (1986).
79. I.M. Kalogeras and W. Brostow, *J. Polym. Sci. Phys.* **47**, 80 (2009).
80. I.M. Kalogeras, *Thermochim. Acta* **509**, 135 (2010).
81. I.M. Kalogeras, *Eur. J. Pharm. Sci.* **42**, 470 (2011).
82. L.A. Pfister, and Z.H. Stachurski, *Polymer* **43**, 7419 (2002).
83. R.M. Dammert, S.L. Maunu, F.H.J. Maurer, I.M. Neelov, S. Niemelä, F. Sundholm and C. Wästlund, *Macromolecules* **32**, 1930 (1999).
84. T.G. Fox and P.J. Flory, *J. Appl. Phys.* **21**, 581 (1950).
85. M.D. Shelby, A.J. Hill, M.I. Burgar and G.L. Wilkes, *J. Polym. Sci. Phys.* **39**, 32 (2001).
86. G.N. Toepperwein and J.J. de Pablo, *Macromolecules* **44**, 5498-5509 (2011).
87. I.M. Kalogeras, "*Contributions of Dielectric Analysis in the study of nanoscale properties and phenomena in polymer*s", in: *Progress in Polymer Nanocomposite Research* (eds. S. Thomas, G. Zaikov), Chapter 10, pp. 253-309, Nova Science (2008).
88. V.V. Novikov, C. Friedrich, N.O. Dmitrieva and A.V. Novikov, *Sci. Eng. Comp. Mater.* **16**, 21 (2009).
89. K. Li, X.L. Gao, J.C. Fielding and T.B. Tolle, *J. Comput. Theor. Nanosci.* **6**, 494 (2009).
90. C.J. Capozzi, Z. Li, R.J. Samuels and R.A. Gerhardt, *J. Appl. Phys.* **104**, 114902 (2008).
91. S. Gupta, R. Ou and R.A. Gerhardt, *J. Electron. Mater.* **35**, 224 (2006).
92. L.E. Levine, G.G. Long, R.A. Gerhardt, R. Ou, J. Ilavsky and C.A. Parker, *Appl. Phys. Lett.* **90**, 014101 (2007).
93. T. Kondo and K. Tsumuraya, *J. Chem. Phys.* **94**, 8220 (1990).
94. P. Jund, D. Caprion and R. Jullien, *Europhys. Lett.* **37**, 547 (1997).
95. H.G.E. Hentschel, V. Ilyin, N. Makedonska, I. Procaccia and N. Schupper, *Phys. Rev. E* **75**, 050404(R)

(2007).

96. E. Aharonov, E. Bouchbinder, V. Ilyin, N. Makedonska, I. Procaccia and N. Schupper, *Europhys. Lett.* **77**, 56002 (2007).
97. B. Doliwa and A. Heuer, *Phys. Rev. E* **67**, 031506 (2003).
98. A. Heuer, *J Phys.: Condens. Matter* **20**, 373101 (2008).
99. T.S. Jain and J.J. de Pablo, *Phys. Rev. Lett.* **92**, 155505 (2004).
100. T.S. Jain and J.J. de Pablo, *J. Chem. Phys.* **122**, 174515 (2005).
101. F.H. Stillinger and T.A. Weber, *Phys. Rev. A* **28**, 2408 (1983).
102. M. Goldstein, *J. Chem. Phys.* **51**, 3728 (1969).
103. C. Grufman and F. Ellyin, *Comp. Sci. Technol.* **67**, 766 (2007).
104. S. Ghosh, Z. Nowak and K. Lee, *Acta Mater.* **45**, 2215 (1996).
105. T.G. Stange, R. Mathew, D.F. Evans and W.A. Hendrickson, *Langmuir* **8**, 920 (1992).
106. L.L. Song, V. Sharma, J.O. Park and M. Srinivasarao, *Soft Matter* **7**, 1890 (2011).
107. R.J. Babu, W. Brostow, O. Fasina, I.M. Kalogeras, S. Sathigari and A. Vassilikou-Dova, *Polym. Eng. Sci.* **51**, 1456 (2011).
108. W. Brostow, R. Chiu, I.M. Kalogeras and A. Vassilikou-Dova, *Mater. Lett.* **62**, 3152 (2008).
109. Q. Yin, J.-H. Luo, G. Zhou, Q.-J. Yin and B. Jiang, *Molec. Simulat.* **36**, 186 (2010).
110. D.-X. Li, B.-L. Liu, Y.-S. Liu and C.-L. Chen, *Cryobiology* **56**, 114 (2008).
111. E. Karavas, E. Georgarakis and D. Bikiaris, *J. Thermal Anal. Cal.* **84**, 125 (2006).
112. F.W. Starr, S., Sastry F.J., Douglas and S.C. Glotzer, *Phys. Rev. Lett.* **89**, 125501 (2002).
113. http://www.personal.kent.edu/~rmuhamma/Compgeometry/compgeom.html
114. http://www.cs.cornell.edu/home/chew/Delaunay.html
115. http://www.pollak.org/en/otherstuff/voronoi/
116. http://www.raskob.de/fun/d/index-en.php
117. http://www.pi6.fernuni-hagen.de/GeomLab/VoroGlide/index.html.en
118. http://www.cs.uiuc.edu/~jeffe/compgeom/demos.html
119. http://math.lbl.gov/voro++/
120. http://pages.cpsc.ucalgary.ca/~marina/vpplants/
121. http://www.righto.com/fractals/vor.html
122. http://www.wblut.com/2008/04/01/voronoi-fractal/
123. http://www.voronoigame.com/